Gold-induced faceting on a Si(001) vicinal surface: Spot-profile-analyzing LEED and reflection-electron-microscopy study

H. Minoda* and K. Yagi
Department of Physics, Tokyo Institute of Technology, Oh-okayama, Meguro, Tokyo 152, Japan

F.-J. Meyer zu Heringdorf, A. Meier, D. Kähler, and M. Horn von Hoegen
Institut für Festkörperphysik, Universität of Hannover, Appelstrasse 2, D-30167 Hannover, Germany
(Received 29 December 1997; revised manuscript received 15 July 1998)

Au-induced faceting on a 4° off Si(001) vicinal surface at temperatures between 750 and 880 °C was studied by *in situ* high-resolution low-energy electron diffraction and ultrahigh vacuum reflection electron microscopy. The formation of an Au-induced incommensurate 5×3.2 reconstruction on (001) terraces triggers the transformation of the initial regular step train of the vicinal surface into a ''hill-and-valley'' structure composed of very wide (001) terraces and step bands. With further increasing Au coverage the step bands transform to well-ordered (119) facets, which also exhibit the Au-induced reconstruction. For adsorption temperatures below 800 °C the transformation to the well-ordered (119) facet is kinetically hindered: an irregular mixture of (115), (117), and (119) facets is observed. The (001) terraces and facets are alternately arranged to form a hill-and-valley structure with an average period of ~400 nm and terrace lengths of more than several hundreds of μm. Driving force for the large-scale morphological transformation into the hill-and-valley structure is the decrease of surface free energy of the (001) and the (119) surface due to the formation of Au-induced reconstruction on (119) facets as well as on (001) areas. [S0163-1829(99)03503-1]

I. INTRODUCTION

Si surfaces show a variety of different surface reconstructions depending on temperature and the crystallographic orientation. Driving force for the formation of the surface reconstruction is the minimization of surface free energy, which is very often identical with a reduction of the number of dangling bonds. Adsorption of foreign elements reduces the surface free energy and it strongly modifies the electronic structure at the surface. Therefore, this process is always accompanied by a change of surface structure, which may lift the surface reconstruction or change the surface unit cell.

Metal-induced surface reconstructions on low-index Si surfaces, such as (111), (001), and (110), have been extensively studied as function of substrate temperature and amount of adsorbed metals.[1] However, on vicinal surfaces, the steps and step-step interactions also play a significant role for the apparent surface morphology. Metal adsorption modifies not only the surface free energy of the various kinds of planes, but also the step free energy and the step-step interaction. All of this together may cause a significant breakup of a smooth vicinal surface into a ''hill-and-valley'' structure composed of large, flat low index planes and areas where all the steps are accumulated. The steps may either form irregular highly inclined step bunches (step bands) or well-ordered facets with a distinct orientation. Such a hill-and-valley structure is stabilized by the adsorbate induced reconstruction on both the low-index plane and the high-index facet plane formed to conserve the macroscopic miscut of the sample. Under equilibrium conditions the surfaces with low surface energies are considered to grow and very wide step free areas can form, depending on the diffusion and mobility of the Si adatoms (which additionally may be affected by the metal adsorption[2]). Metal-induced step bunching and/or faceting are very attractive and interesting not only from a scientific point of view but also as a new technique for self-organized formation of low-dimensional surface morphologies and structures without lithographic processes.

Recently, several studies have been carried out in the field of noble-metal-induced step bunching or faceting of vicinal semiconductor surfaces.[3–8] Some of the results were obtained by reflection electron microscopy and diffraction (REM-RHEED).[6,7] Aoki *et al.* found formation of (335) facets by Au deposition on a Si(111) vicinal surface at approximately 780 °C.[6] Au adsorption on a Si(hhm) surface ($m/h = 1.4-1.5$) at approximately 700 °C results in the formation of the hill-and-valley morphologies consisting of (557), (335), (225), and (113) facets in addition to (111) faces depending on the Au coverage.[7] (5 5 11) and (441) facets are formed when Au is adsorbed on (5 5 12) and (331) surfaces,[7] respectively. These surfaces are not stable as bare Si surfaces,[9] i.e., are only stabilized by Au adsorption. Some of the Au-induced facets disappear with increasing temperature at 740–820 °C. These reversible transitions are considered to be roughening transitions with a transition temperature depending on facet orientation.[7]

The formation of an Au-induced surface reconstruction plays a very important role for Au-induced faceting of Si(111) as studied by scanning tunneling microscopy (STM).[4] Au adsorption stabilizes Si(775) and Si(995) surfaces. Both surfaces are unstable without Au and were not observed by REM-RHEED on clean cylindrical sample.[9] The STM study reveals the Si(775)-Au surface composed of very narrow (111) terraces together with surface steps. The (111) terraces show a similar structure of a Si(111)5×2-Au surface reconstruction. The width of the narrow terraces in the Si(775) facet corresponds to the width of the unit cell of the

surface reconstruction. The Si(775)-Au facet is, therefore, formed by a regular array of very narrow Si(111) terraces separated by atomic bilayer steps. Only the formation of a well-defined reconstruction on the single terraces of the Si(775) high index facet stabilizes this complex structure.

Si(111) surface structure is not particularly anisotropic neither is the surface diffusion of adatoms. In contrast Si(001) surfaces are remarkably anisotropic in the surface reconstruction, the surface tension and the atomic step structure and step-step interaction. From this results a strong anisotropy for the surface diffusion of adatoms on terraces[10] and along steps. On Si(001)-(2×1) surfaces with small miscut with the dimers oriented orthogonal directions reconstructed (2×1) and (1×2) domains exists. On the other hand on Si(001) surfaces with large miscut (larger than 4° inclined to the $\langle 1\bar{1}0\rangle$ direction) one orientation domain exists on the individual terraces which are separated by an regular array of double height steps (D_B steps). This configuration is more stable than an alternative array of single height steps (S_A and S_B steps).[11–13] On a 4° off vicinal surface inclined to the $\langle 1\bar{1}0\rangle$ direction we expect a very pronounced anisotropic surface diffusion of adatoms during the adsorption of Au. On this surface dimer rows run parallel to the miscut direction with a faster surface diffusion in this direction. This anisotropy may strongly enhance changes of surface morphology during metal adsorption.

We have observed Au-induced faceting on a 4° vicinal Si(001) surface by using REM-RHEED, spot profile analyzing low-energy electron diffraction (SPA-LEED), atomic force microscopy, and light scattering.[14] SPA-LEED and REM-RHEED studies are presented in this paper.

II. EXPERIMENTAL

The experiments were performed in a standard ultrahigh vacuum (UHV) chamber with base pressure of 1×10^{-8} Pa equipped with a SPA-LEED system and an ultrahigh vacuum electron microscope (UHV-EM) equipped with an Au evaporator and a thickness monitor.[15] Si samples were cut from a (001) wafer with a misorientation of 4° towards $\langle 1\bar{1}0\rangle$ (Wacker Chemitronic, *u* type). After degassing at 650 °C for 24 h the samples were flashed to 1200 °C to remove the native oxide. The formation of a single domain surface with a periodic double step train was always observed (see Fig. 1). Au was deposited at temperatures in between 750 and 845 °C, using a deposition rate of about 0.1 ML/min.

LEED spot profiles were monitored during deposition of Au using a second electron gun in a grazing geometry.[16] This allows following the evolution of surface morphology during Au adsorption. Usually spot profiles along the miscut direction (the $\langle 1\bar{1}0\rangle$ direction) were successively measured during the deposition of Au at high temperatures using the secondary electron gun (see Figs. 7, 8, and 13). Two-dimensional 2D LEED patterns were taken after quenching to room temperature RT (see, Figs. 1, 2, and 12). In all 2D pattern shown in this paper the miscut direction of the sample corresponds to the horizontal axis.

The miscut direction of the sample for REM has been chosen to be parallel to the elongated side of the sample, i.e., in the micrograph the electron beam (close to the $\langle 1\bar{1}0\rangle$ direction) incident along the steps. All REM images are distorted by a foreshortening factor of 1/40 along the electron beam direction because the electron beam is incident under grazing angle.

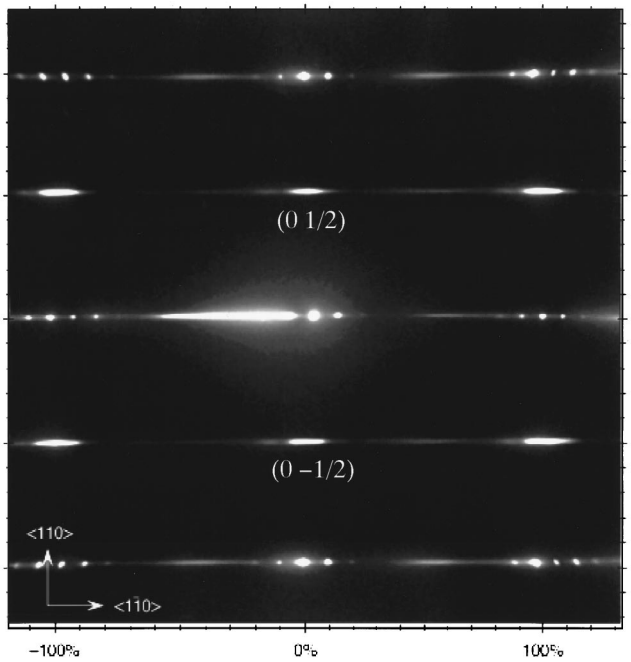

FIG. 1. LEED pattern from a bare 4° vicinal Si(001)(1×2) surface in a logarithmic intensity scale to show also weak details in the background. Miscut of the sample is along $\langle 1\bar{1}0\rangle$. Single domain structure is apparent. The very regular step train results in a spot splitting of all integral order spots. Incident electron beam energy was 80 eV.

After chemical cleaning the sample crystals were clamped with two electrodes of a sample holder of the microscope. After introduction of the sample crystal into the column chamber of the microscope, a native oxide of the sample was removed by dc current heating at 1200 °C. Au was deposited from a tungsten wire at substrate temperatures of 800–880 °C at a deposition rate of about 3 ML/min in Figs. 6 and 14–16 (0.5 ML/min in Fig. 9). After Au deposition the sample temperature was usually decreased to 700 °C to avoid loss of Au from the surface due to desorption and/or diffusion into the Si bulk. REM images were taken at this lower temperature.

III. RESULTS AND DISCUSSION

A. Surface reconstructions

The LEED pattern of the bare Si(001) vicinal surface before Au adsorption is shown in Fig. 1. The electron energy was 80 eV with a diffraction condition close to the second Bragg condition (008), which corresponds to a scattering phase $S=2$ or an electron energy $E=82$ eV. Under this condition electrons from neighboring terraces interfere constructively (in-phase condition). The regular array of the step train becomes apparent in the spot splitting of any integral order spot. The grid of perfectly arranged steps acts as a phase grid

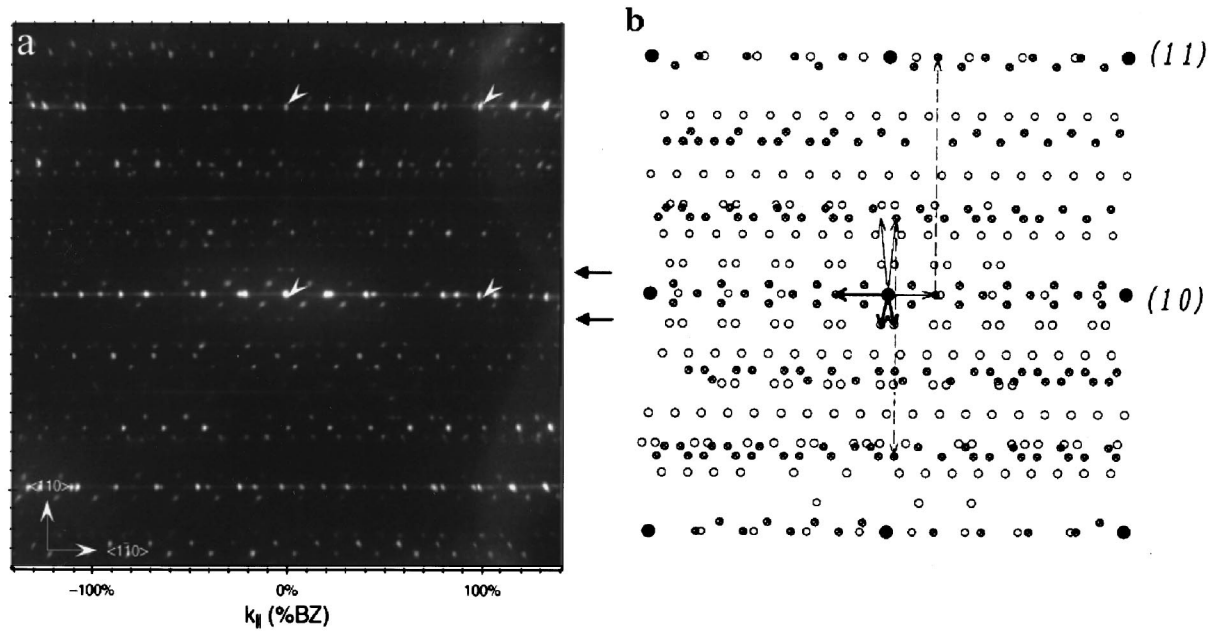

FIG. 2. (a) LEED pattern taken at RT after Au-induced faceting at 800 °C. Spots result from 5×3.2 reconstruction on (001) terraces and 8×2 reconstruction on (119) facets. The electron energy was 39 eV. (b) A Schematic illustration of the LEED pattern. Solid circles are integral order spots from the Si(001) lattice, hatched circles are spots are from 5×3.2 reconstruction on the (001) areas, and open circles are the spots originating from the (119) facet with 8×2 reconstruction.

for electrons which results in a splitting of all spots, which is reciprocal to the separation between neighboring steps. The spot splitting of 10% of the surface Brillouin zone (here the distance to the next integral order spot) indicates a terrace width or step separation of 4 nm, i.e. the existence of double height steps.

Superlattice spots from the (1×2) reconstruction indicated by (0 1/2) and (0 −1/2) are also clearly seen. The weak intensity of the (2×1) spots reflects the formation of an almost perfect single domain structure with the dimer rows of the major (2×1) domains parallel to the miscut direction and D_B type steps.

Au adsorption at 800 °C results in the 2D LEED pattern shown in Fig. 2(a) after quenching the sample to room temperature. A schematic illustration of the LEED pattern is given in (b). Vertical arrows in (a) indicate the integral order (00), (10), and (11) spots from the Si(001) surface. The large number of additional spots arises from complex reconstructions on flat Si(001) terraces and facets. The spots from the initial LEED pattern of the step train of the 4° off vicinal surface are no longer visible. In (b), solid circles indicate the integral order spots of the bulk terminated Si(001)1×1 surface and hatched circles indicate spots arising from the Au-induced surface reconstruction on the (001) surface. Open circles correspond to spots from the Au-induced surface reconstruction on the facets.

The first set of superlattice spots (hatched circles) show a well-defined fivefold periodicity with respect to the distance between integral order spots along the miscut $\langle 1\bar{1}0\rangle$ direction. This indicates that these spots arise from a reconstruction on the Si(001) surface. The basic reciprocal vector in the $\langle 1\bar{1}0\rangle$ direction is (1/5 0) which is indicated by a horizontal thin arrow in Fig. 2(b). The second basic reciprocal vector of the reconstruction unit cell was found to be one of two upward thin arrows in Fig. 2(b). Due to the mirror symmetry of the crystal in the vertical line in Fig. 2(b), two equivalent orientational domains are possible. All spots (the hatched circles) could be constructed by using these two sets of basic reciprocal vectors together with a multiple scattering process using the integral order spots of the Si(001) face.

From these vectors the unit cell of the Au-induced surface reconstruction on Si(001) is derived as an incommensurate (5×3.2) structure with one basic reciprocal vector rotated by 5.7°, which will be referred to as 5×3.2. This structure seems to be similar to the Au-induced $(\sqrt{26}\times3)$ and the (5×3) structures already found on Si(100).[17–19] However, it must be pointed out that both of these structures show LEED patterns which are different from the pattern shown here.

The unit cell in real space of the complex 5×3.2 structure is illustrated in Fig. 3 on a (1×1) unit mesh. From the LEED pattern shown in Fig. 2(a), it is obvious that no rotational 3.2×5 domain exits. The 5×3.2 reconstruction exits also in a twisted domain with the mirror plane perpendicular

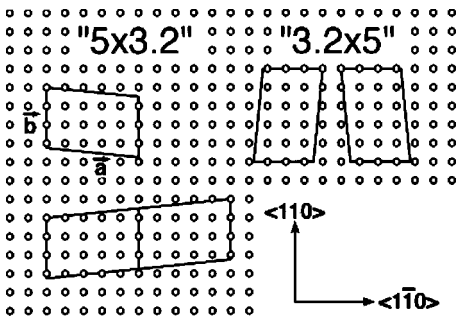

FIG. 3. A schematic illustration of the unit cell of the (001)5 $\times$3.2-Au surface and its mirror domain. The 90° rotated domains are also shown.

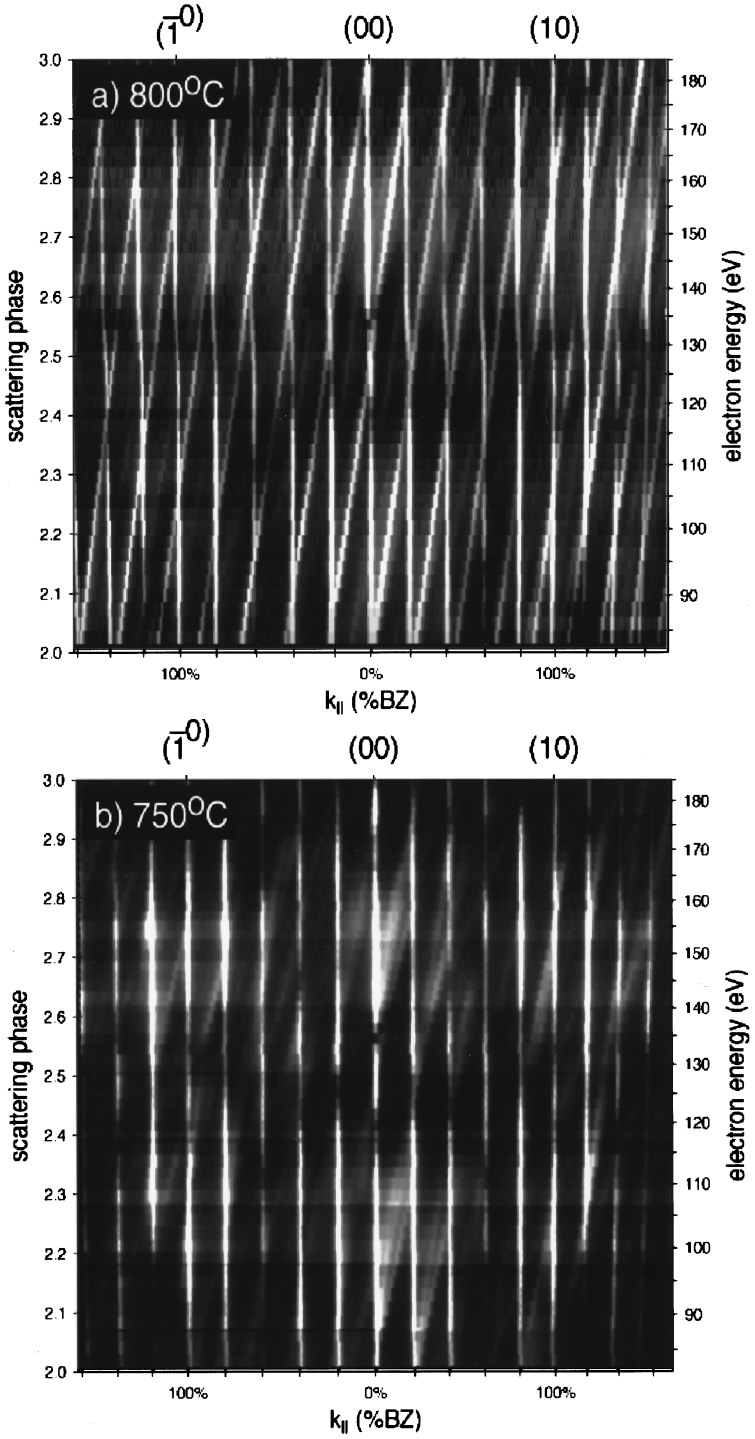

FIG. 4. Spot profiles along the $\langle 1\bar{1}0 \rangle$ direction from LEED patterns (as shown in Fig. 2 at various energies) are plotted in a gray-scale representation as a cut through reciprocal space. The vertical bright lines are reciprocal lattice rods from integral order spots and from 5 $\times$3.2 reconstruction spots. Tilted lines correspond to tilted areas at the surface, i.e., reflect the movement of facet spots in reciprocal space as a function of electron energy. (a) Au adsorption at 750 °C results in formation of various kinds of facets [the (115), (117), and (119) facets. (b) Au adsorption at 750 °C results in the formation of solely (119) facets.

to the miscut direction as also shown in Fig. 3. The initial surface prior to Au adsorption showed a (1×2) reconstruction so the 5×3.2 domains are formed on the 1×2 domains.

The second set of spots is indicated by open circles in Fig. 2(b) and belongs to an Au-induced commensurate reconstruction on a facet plane. The facet plane could be easily determined from the variation of facet spot position in reciprocal space as function of the vertical scattering vector. This has been done by recording spot profiles along the $\langle 10 \rangle$ direction for various incident electron energies from 82 eV [$S=2$ or (008) Bragg condition] to 180 eV [$S=3$ or (0,0,12) Bragg condition]. Such profiles are depicted in Fig. 4 as a vertical cut in reciprocal space with k_{II} as the x axis and $k_{\perp}$ as the y axis.

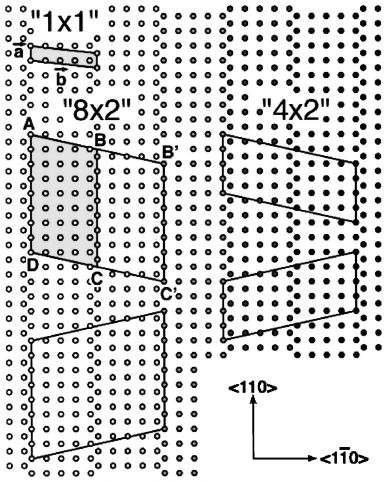

FIG. 5. Schematic illustration of the unit cells of the 8×2 (left) and the 4×2 (right) structures on the (119) surface. The primitive (119) unit cell is labeled 1×1.

Figures 4(a) and 4(b) reproduce plots of LEED intensity distributions along the $\langle 1\bar{1}0\rangle$ direction after Au deposition at 750 and 800 °C, respectively. In (b) the vertical lines correspond to the spots (or reciprocal lattice rods) from the (001) surface with the 5×3.2 reconstruction. There are four additional spots in between integral order spots. Now the movement of the facet spots with respect to the stationary spots of the (001) areas becomes obvious in the lines running in oblique directions. From their inclination and the intersection with the (001) rods, a (119) facet orientation is easily derived. Both the facet rods and (001) rods show no broadening, which reflects a perfect order on a scale larger than the transfer width of 100 nm of the instrument.

For adsorption at lower temperatures three kinds of oblique lines are seen in Fig. 4(a) in addition to the vertical lattice rods from the (001) surface. One corresponds to a (119) facet as in (b) and the others are from (117) and (115) facets. Here the facet rods are much broader and more diffuse with a lower intensity than those in (b) (Au was deposited at higher temperatures). This means that the facets in (a) are smaller than those in (b). It should be noted that in the temperature range between 750 and 800 °C (115), (117), and (119) facets are formed, although at lower temperature the facets are not well developed. For adsorption temperatures above 800 °C only (119) facets are formed. In no case was the formation of only (117) facets observed.

The superlattice reflections indicated by open circles in Fig. 2(b) are from (119) facets. The length of the basic reciprocal vector in $\langle 1\bar{1}0\rangle$ direction is $\frac{2}{9}$ of the reciprocal vector of the bulk terminated (001) surface. This reflects the formation of (119) facets with double step structure sketched as a 1×1 unit cell in Fig. 5. Narrowly spaced $\frac{1}{8}$th-order reflections can be seen along the horizontal lines indicated by horizontal arrows in Fig. 2(a). This reflects the formation of an eight-fold structure on the (119) facets in the $\langle 110\rangle$ direction. The unit cell vectors in reciprocal space are plotted as horizontal thick arrows to the left and one of the two short downward arrows in Fig. 2. The resulting real space unit cells for the possible reconstructions on the (119) facet are shown in the left of Fig. 5 as parallelogram *ABCD*. Because

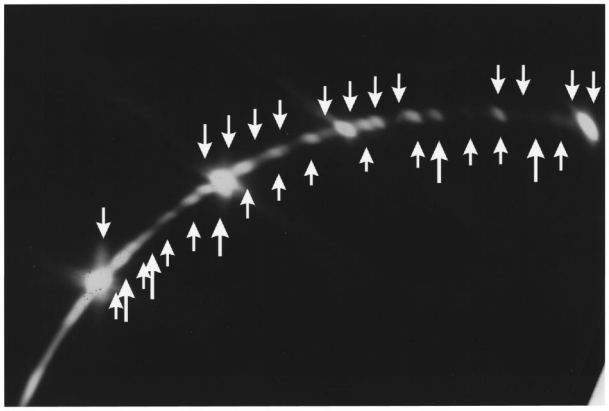

FIG. 6. RHEED pattern taken after the Au adsorption at 800 °C. Diffraction spots from the (001) terraces with the 5×3.2 structure are marked by downward arrows, (119) facet spots by large upward arrows, and (117) facet spots by small upward arrows.

the positions *A* and *B* are not equivalent positions on the (119) surface the unit cell of the surface reconstruction on the (119) surface should be taken as the larger parallelogram $AB'C'D$. The superlattice structures indicated by the solid lines are described in matrix notation as

$$\begin{pmatrix} 2 & 1 \\ 0 & 8 \end{pmatrix}$$

with mirror domain. For simplicity, we will describe this structure as the ''8×2'' structure. Depending on details of the adsorption process sometimes a 4×2 structure, in the matrix notation the

$$\begin{pmatrix} 2 & 1 \\ 0 & 4 \end{pmatrix}$$

and its mirror domain has been observed as shown in Fig. 5 right. Instead of an eightfold periodicity in the $\langle 110\rangle$ direction a fourfold periodicity is observed. It is not clear which details of the adsorption process determines the formation of the fourfold or eightfold periodicity.

In contrast to the strict appearance of the reconstruction on the (119) facet we have never observed a surface reconstruction on the (117) facets in any of the LEED patterns. As mentioned before the (119)-Au surface is considered to be more stable than the (117)-Au surface. This is mainly due to the fact that Au-induced surface reconstructions are formed on the (119) surface.

Reflections from superlattice structure on the (001) terraces and facets were also observed by RHEED. Figure 6 reproduces the RHEED pattern after deposition of Au at 830 °C. The pattern was taken at a temperature of about 700 °C. Reflections indicated by downward arrows results from the 5×3.2 structure on the (001) surface. Between integral order spots four additional and equidistant spots are present indicating that the fivefold direction of the 5×3.2 structure runs parallel to the miscut direction and perpendicular to the step edges. The initial surface shows a single domain structure with the twofold direction of the 2×1 structure perpendicular to the miscut direction. Thus, the 5×3.2 domains form on the 1×2 domains.

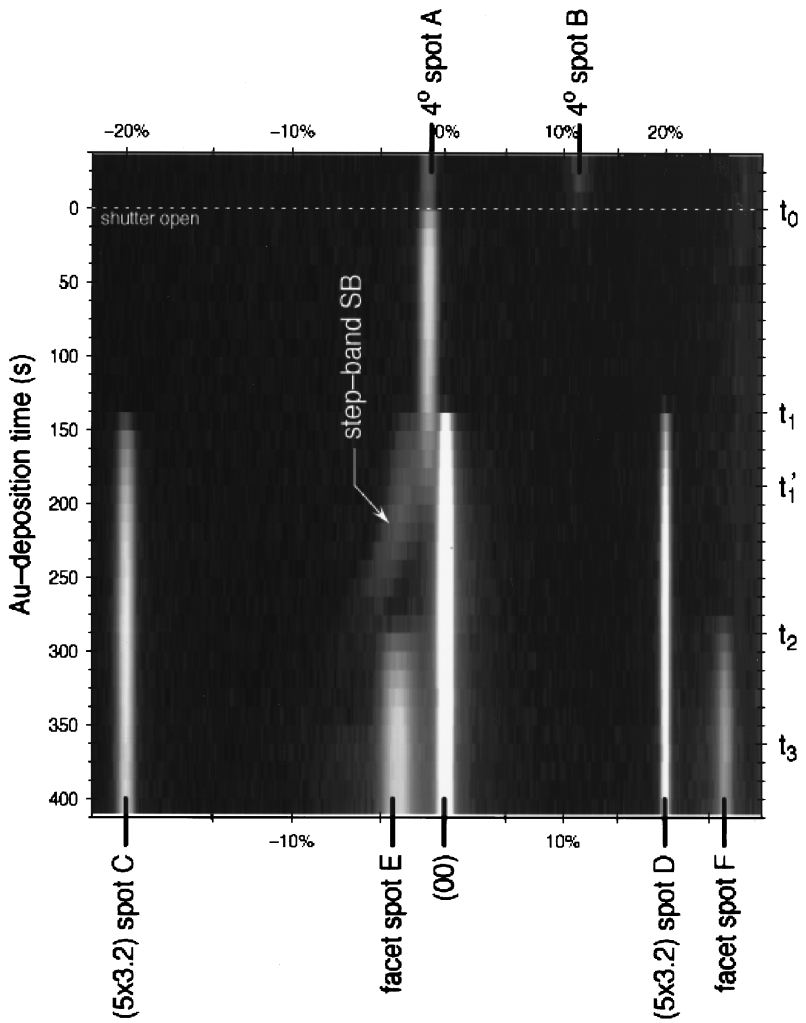

FIG. 7. The kinetics of the faceting process is studied during Au adsorption by recording LEED intensity profiles along $\langle 1\bar{1}0\rangle$ direction. The profiles are shown as a function of adsorption time in a logarithmic gray-scale representation. Top line represents the initial 4° off step train, the last line the formation of a hill-and-valley structure with various different spots originating from (001) terraces and facets. Due to grazing incidence the LEED pattern is distorted, which causes the different scales of the *x* axis.

In addition to the reflections from the 5×3.2 structure, reflections from (119) and (117) facets are seen in the RHEED pattern and are indicated by large and small upward arrows, respectively. Thus, (119) and (117) facets are formed on the surface by Au adsorption in accordance with the SPA-LEED study.

B. Kinetics of morphological transition

The large-scale morphological transformation of a regular stepped (1×2) reconstructed Si(001) vicinal surface into a hill-and-valley structure composed of alternatively arranged (001) terraces and (119) facets has been studied by *in situ* SPA-LEED measurements using an external electron gun with a grazing incidence of 30°. Continuous recording of spot profiles along $\langle 1\bar{1}0\rangle$ direction during Au adsorption allows following a change of surface morphology in detail. An electron energy of $E=96$ eV corresponds to a phase condition of $S=0.95$ for external geometry, which allows to easily separate facets with different orientations, flat (001) areas, and differently inclined step bands. This is impossible for the in-phase condition at $S=1$, where all spots collapse at the (004) Bragg condition.

The changes in the spot profiles during Au adsorption are shown in Fig. 7 in a gray-scale representation with the *x* axis for k_{II} and the downward axis corresponding to the deposition time. Changes of the intensity distribution, in other words, changes of the surface morphology during Au deposition can be divided into four stages as follows.

Stage 1. From t_0 to t_1. The split (00) spots originating from the 4° vicinal surface is seen before Au deposition and denoted by spots *A* and *B*. The intensity of spot *A* increases at the initial stage of Au deposition. This is probably caused by an increase in reflectivity due to the increased Au coverage on the surface. However, its position and width does not change, which indicates that the surface morphology does not change during this stage although the Au coverage increases almost linearly.

Stage 2. From t_1 to t_1'. Above a critical Au coverage new spots appear very suddenly at t_1. These spots can be attributed to the (00) spot from the flat (001) surface denoted as (00). At the same coverage spots from the Si(001)5×3.2-Au structure arise at positions $+20\%$ and -20% of the surface Brillouin zone (% SBZ) denoted as *C* and *D*. Diffuse intensity indicated as step band (SB) appears to the left of spot *A*.

The horizontal scale for $k_{\|}$ is nonlinear due to the grazing incidence of the electrons in this diffraction geometry.[20] The x scale has been corrected for this distortion. The first nucleation of the flat Si(001) terraces happens at the same coverage as the formation of the 5×3.2 structure. It is concluded that the surface free energy of the (001) areas is reduced due to the formation of the Au-induced reconstruction. Reduction of the surface free energy of the (001) areas is a driving force for the break up process of the vicinal surface into the flat (001) terraces and step bands. The diffuse intensity SB is considered to be from step bands with higher inclination angle than the initial 4° surface.

With increasing Au coverage the intensity of the (00) spot and the spots C and D from the 5×3.2 reconstruction increases, while that of the spots A and B from the 4° initial surface decays and disappears at $t=t_1'$. The position of the diffuse intensity SB does not change at this stage, which means that the average inclination angle of the step bands does not change. From the mean position of the diffuse intensity the inclination angle of the step bands is estimated to be 8°. During this adsorption stage, 4° off vicinal areas are still present and transform into flat wide Si(001)5×3.2 terraces separated by step bands with higher step density.

Stage 3. From t_1' to t_2. With the disappearance of the 4° spot A, the position of the diffuse reflection (SB) gradually and continuously moved away from the (00) spot. This diffuse reflection is considered not to be from the distinct facets but from the step bands. The continuous shift of the position of SB with further Au deposition indicates a continuous increase of the average inclination angle of the step bands from 8° to ~14°. During this motion in the position of the diffuse reflection SB, the intensity of the (00) and the superlattice spots slightly increases and almost saturates at t_2.

Stage 4. from t_2 to t_3. At a second critical coverage ($t=t_2$) the diffuse reflection SB disappears and new spots (indicated by E and F) appear. The intensity of these new spots increases with no change of position during further Au deposition. These new spots are identified as facet spots originating from facets with a distinct (119) orientation. It is surprising that the position of the facet spot in k space does not coincide with the final position of the step band spot SB. This can only be explained by a decrease of the inclination angle of the stepped areas during the faceting process. Although the step bands transform into the facets they are much steeper (~14° inclination) than the resulting (119) facet with 8.9° inclination angle. This overshooting phenomenon will be discussed later. Conservation of the macroscopic miscut of the sample requires that the flat (001) terraces shrink in size during this process, which is observed as a weak decrease in intensity of the (00) spot from t_2 to t_3 (see Fig. 8).

The relative integrated intensities of the different spots in Fig. 7 are plotted on a linear intensity scale as a function of Au deposition time in Fig. 8. The different stages mentioned above can be clearly separated. The sudden onset of a linear increase in the intensity of the (00) spot and the 5×3.2 spots with Au coverage starting at t_1 reflects the formation of reconstructed areas only above the first critical Au coverage and this growth proportional to the additional Au coverage.

Faceting process (after $t=t_2$) can be explained by a similar process to that between t_1' and t_2: above the second critical coverage the facet area increases linearly with increasing Au coverage. At the same time the intensity of the (00) spot and the 5×3.2 spots decreases slightly due to the transformation of steep step bands into smoother facets at the expense of the (001) terraces.

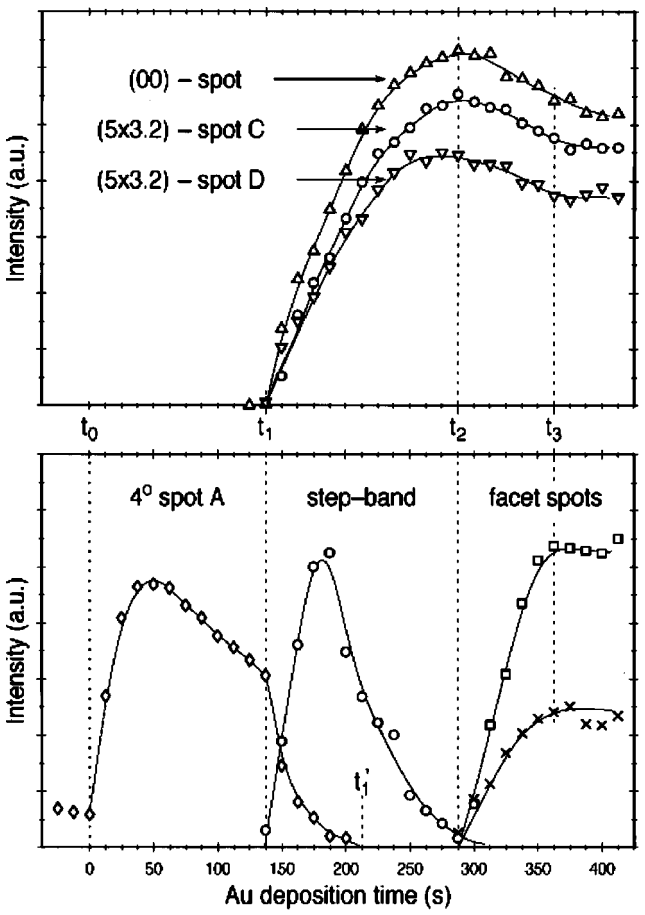

FIG. 8. Temporal changes of the integral intensities of the different spots seen in Fig. 7.

Step bunching and faceting processes were also observed using REM. Figure 9 reproduces a series of REM images recorded on a video tape that show changes in surface morphology during Au deposition at 800 °C at a deposition rate of 0.5 ML/min. The white arrow in (a) points in the direction of the imaging electron beam ($\langle 1\bar{1}0\rangle$ direction). The length of the white bar in (a) is 300 nm and is oriented along the miscut direction ($\langle 110\rangle$ direction). The downward direction of the step train is the lower right part of the image. The images are foreshortened by 1/40 in the direction perpendicular to the scale bar as mentioned in Sec. II. The image (a) was taken during the Au deposition just after the first nucleation of a dark region, which corresponds to a (001)5×3.2 terrace. The surrounding areas have not changed in contrast, which indicates that they still have the step structure of the original 4° off surface. The individual double height steps can not be resolved because the step-step distance of 4 nm (double height step train) is below the resolution limit.

In (b), the (001) terrace visible as dark line (marked by A) nucleates and grows. The shape of terrace A is very anisotropic and it grows preferentially along the direction perpendicular to the miscut direction, i.e., along the step edges. Taking into account the foreshortening factor of 1/40, an

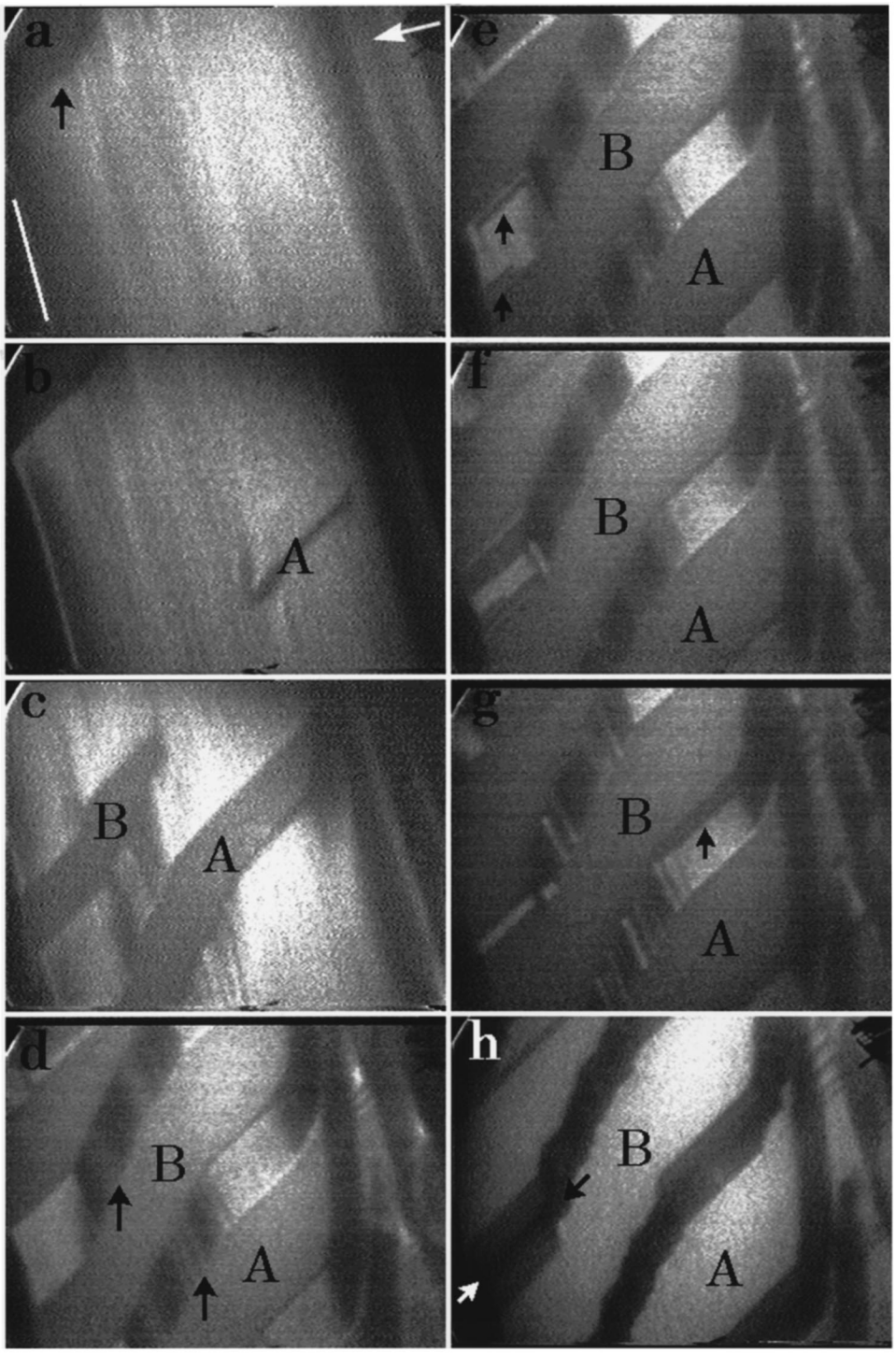

FIG. 9. A series of REM images during the deposition of Au at 800 °C shows first the formation of a (001) terraces (a) and (b). Step bunching and formation of step bands are shown in (c) and (d); facet nucleation on the step bands is shown on (f) and (g). Complete transformation of the entire vicinal surface into a hill-and-valley structure of (001) superterraces and (119) and (117) facets.

aspect ratio of more than 400 results for terrace *A*. Although the field of view in (c) is slightly shifted from that in (b), it is obvious that terrace *A* has grown wider and has a complicated shape. A second (001) terrace—marked by *B*—has nucleated between (b) and (c). Conservation of the number of steps and the overall miscut of the sample requires the formation of a step band between the terraces *A* and *B*: The step density in the step band areas must have increased significantly, which is in very good agreement with the SPA-LEED results. In (d) several step bands are seen between the (001) terraces as indicated by arrows. With increasing Au coverage the (001) terrace become broader resulting in even steeper step bands. The step bunching process has almost finished between image (d) and (e).

With further Au adsorption, nucleation and growth of dark areas is seen in the step bands as indicated by arrows in (e) and (g). The change in contrast in some parts of the step bands indicates a change of reflection condition due to the

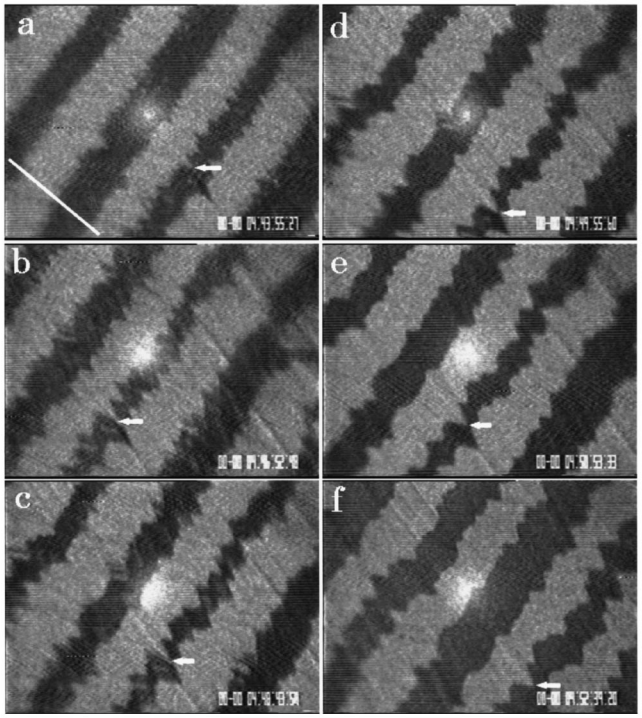

FIG. 10. A series of REM images during annealing and Au desorption reveal the time-reversed process of faceting. The white arrows mark an identical position in each image. The length of scale bar is 300 nm. The (001)-terrace and (119)-facet structure in (a) was obtained at 870 °C. With decreasing Au coverage the facets rearrange to steeper step bands (c) while the (001) terraces increase in width. With further decreasing Au coverage the (001) terraces become unstable and become narrower while the step bands get broader by debunching due to conservation of macroscopic miscut.

nucleation and the formation of well-ordered facets. The nucleation of the facets takes place at the upper and the lower edges of the step bands and they grow larger—as seen from (e) and (f)—at the position indicated by arrows in (e). Finally all the facets increases in size and all step bands are completely transformed to facets in (b). In (b) one of the facets shows two different contrast areas: the middle of the facet area indicated by white and dark arrows is slightly darker than the surrounding areas. As described in Sec. III A both (119), and (117) facets are formed during Au deposition. Therefore, these different contrast areas result from different structure factors for diffraction and reflection conditions in electron imaging and are considered to be either (117) or (119) facets.

The transformation of step bands to facets has been studied in more detail during the desorption process. Because the whole morphological transformation is reversible with respect to the Au coverage, the time-reversed process could be studied without the kinetic limitations that may occur during high Au adsorption flux. Figure 10 shows a series of REM images that reproduces changes of the surface morphology of the hill-and-valley structure during desorption of Au. Prior to this sequence Au was deposited at 870 °C to form the alternative arrangement of (001) super terraces (bright areas) and facets (dark areas). For the desorption experiment the sample temperature was set to 750 °C and was gradually increased to 850 °C while the changes of the (001) terrace in width and facet morphology were observed. The white scale bar in (a) is 300 nm. The field of view changes slightly from (a) to (f) due to thermal drift. Arrows indicate the same position in all images. The well-developed bright and dark bands correspond to large and elongated (001) superterraces and facets. From the similar width of terraces and facets it is concluded, that most of the facets are of (119) orientation.

With increasing temperature, i.e., decreasing Au coverage, the widths of the dark bands decrease and the contrast of the dark areas changes slightly from (a) to (b). This is considered to be due to a decrease of the facet areas due to a transformation from facets to step bands with a higher inclination angle than the facets. At the same time the width of the flat (001) terraces increases. By further annealing (or with decreasing Au coverage) the dark bands also change their shape and are more smooth and rounded in (c) and (d). This may be due to the fact that the facets have completely transformed into step bands, which are not so well oriented. In (c) the step bands are the narrowest, the inclination angle has changed from 8.9° for the (119) facet to 12° for the step bands, as estimated from the ratio of bright to dark areas. It is important to note that the slope of the facets is smaller than the maximum slope of the step bands. This behavior is attributed to the formation of an energetically favored well ordered (119) facet, which additionally decreases the surface energy by formation of a reconstruction. This also implies that the surface free energy of the step bands is much higher than that of the flat $(001)5\times3.2$ terraces and that of the well-ordered (119) facet.

With further decreasing Au coverage the flat (001) terraces start to shrink and the step bands get wider. The flat (001) terraces are stabilized only by the Au-induced 5×3.2 reconstruction. The LEED experiments show a linear dependence of (001) areas with Au coverage above the first critical coverage necessary for the formation of the 5×3.2 reconstruction. Therefore, the (001) terraces decreases in width with decreasing Au coverage during desorption as seen in (d)–(f). The inclination angle of the step bands decreases and slowly approaches the macroscopic miscut angle of the vicinal surface.

Figure 11 schematically illustrates the changes of surface morphology during Au adsorption. Figure 11(a) shows the 4° off vicinal surface at t_0. Above the first critical Au coverage at t_1 Au-induced reconstructed (001) areas appear together with narrowly spaced steps (SB) as shown in (b). At t_1' 4° vicinal regions disappear due to the expansion of the (001) terraces. All steps are accumulated in step bands. During stage 3 the expansion of the (001) surfaces causes a further increase of the slope of the step bands as seen in (c). Finally at t_2 (119) facet planes are formed being accompanied by a slight decrease of the (001) terrace areas.

A LEED pattern taken after the onset of the step band formation between t_1 and t_2 reveals a more complex situation: beside the formation of the 5×3.2 reconstruction also a 90° rotated 3.2×5 reconstruction is observed in Fig. 12. Strong superlattice spots with fivefold periodicity are not only seen along horizontal lines (in $\langle 1\bar{1}0\rangle$ direction) between the integral order spots but also along vertical lines along the $\langle 110\rangle$ direction. The intensities of the spots of the rotated domain are almost the same as those of the majority domain. This implies the nucleation of two rotational do-

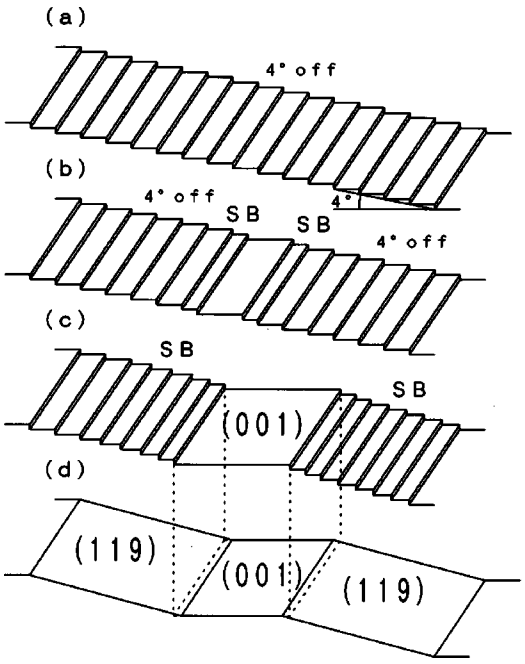

FIG. 11. Schematic illustrations showing the four stages during the transition of the surface morphology. The nucleation and growth processes of the step bands and the facets are shown.

mains (together with their twins) during the early stage of step bunching. However, the minority domain 3.2×5 is no longer present at the end of the adsorption process, when the whole surface was transformed to a single domain 5×3.2 reconstruction on the terraces.

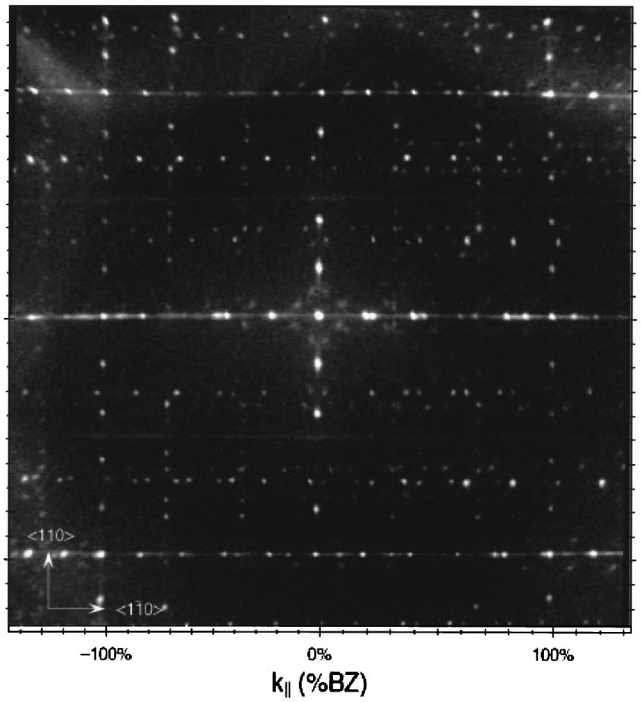

FIG. 12. Temporal changes of the intensity distribution of the LEED pattern along the $\langle 10\rangle$ direction (a) and the $\langle 01\rangle$ direction (b) during the deposition of Au at 800 °C. [It should be mentioned that due to a reversed specimen clamping the horizontal direction to the left in (a) corresponds to the right in Fig. 6.]

The kinetics of the formation and annihilation of the minority domain has again been studied with LEED. Figure 13 reproduces temporal changes of the LEED spot profile during the deposition of Au at 800 °C, (a) along the $\langle 1\bar{1}0\rangle$ and (b) along the $\langle 110\rangle$ direction with the (00) spot in the center. The LEED spot profiles in the two directions were measured alternately. The incident electron energy was 73 eV ($S=0.9$). The scales of the x axis in (a) and (b) are not the same,[20] while those of the vertical axis (time) are identical.

The temporal behavior shown in (a) is similar to that in Fig. 7. An increase of intensity of the spot from the 4° off vicinal surface, appearance of the $(001)5\times3.2$ domains together with an appearance and an increase of step bands, an increase of the average angle of the step bands, and finally, the formation of the facets are noted. Due to a higher deposition rate (than in Fig. 7) facet spots with two different orientations are apparent in the pattern and correspond to (119) and (117) facets, respectively. First the (119) facet is observed, formation of the weaker (117) facet happens at slightly higher coverage. This implies a higher critical coverage for the formation of (117) facets compared with (119) facets.

The pattern in (b) is quite different from that in (a). At the very beginning no spot was observed, because the LEED profile was taken perpendicular to that in (a) at a position in reciprocal space where no spots of the initial vicinal surface are present (see Fig. 1). At t_1 the (00) spot from the (001) areas appears. At slightly higher coverage a superlattice spot of the 3.2×5 minority domain appears (due to image distortions only the spot at $+20\%$ SBZ is observed, the LEED profile does not intersect the spot at -20% SBZ). Its intensity, though much weaker than that in (a), increases up to t_2 and disappears towards the end of the adsorption process. From a comparison of the time scale in (a) and (b), it is concluded that the increase and the decrease of the intensity of the 3.2×5 spots takes place during step bunching and facet formation processes, respectively. It should be noted that the initial surface forms a single domain structure with (1×2) majority domains (dimer rows are parallel to the miscut direction). The present observation indicates that after t_1, the initial 1×2 single domain structure is partially destroyed by the nucleation of all possible major 5×3.2 and minor 3.2×5 domains. During the facet formation processes after t_2 the minor 3.2×5 domains are annihilated, resulting in the 5×3.2 single domain structure shown in Fig. 2.

C. Morphology of the hill and valley structure

Figure 14 shows the surface morphology after Au deposition and phase separation of the vicinal surface into the flat (001) areas and the facets at different temperatures between 800 °C and 880 °C. The direction of the incident electron beam ($\langle 1\bar{1}0\rangle$ direction) is vertical and the miscut direction ($\langle 110\rangle$ direction) is horizontal in each image. At all adsorption temperatures bright and dark areas are visible. Due to a bright field imaging condition the bright areas correspond to the flat Si(001) terraces and the dark areas to the facets, which is confirmed as follows: In Fig. 15 the same area is

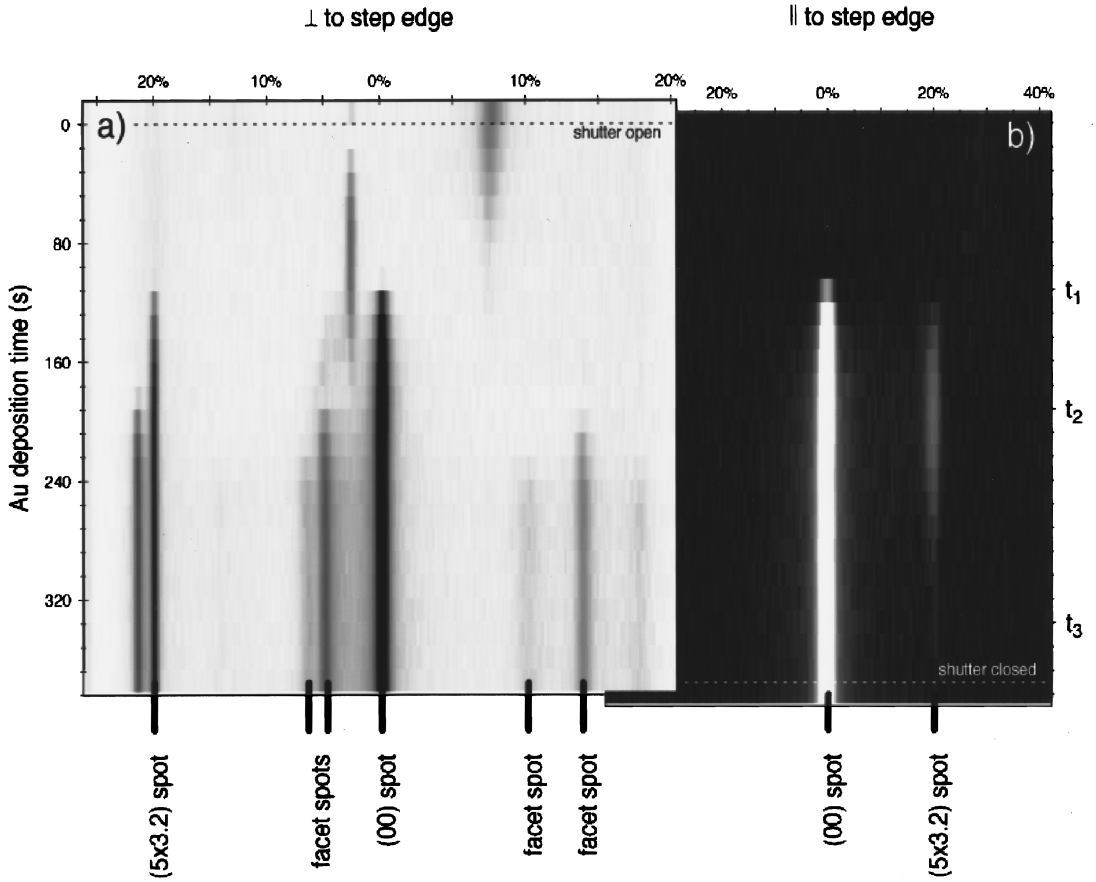

FIG. 13. 2D LEED pattern taken at RT after nucleation of Si(001)5×3.2-Au surfaces at 800 °C during the Au deposition. Incident electron beam energy was 82 eV.

imaged by using (a) the specular reflection and (b) the (1/5 0) reflection from the Si(001)5×3.2 structure. An arrow in (a) indicates the direction of the incident electron beam. The dark scale bar in (a) corresponds to a length of 300 nm. The field of view in (b) is slightly shifted from that in (a) due to a thermal drift and arrows indicate the same rhombic area. The shapes of the rhombus are slightly different from each other due to different imaging conditions. It should be pointed out that bright areas in (a) are also observed as bright areas in (b), which means that these areas under bright field conditions (using the specular beam) correspond to (001)5 ×3.2 terraces.

The facets observed as dark areas in Fig. 14 are considered to be the well-ordered Si(119)-Au and Si(117)-Au facets. Therefore the images clearly show the phase separation of a smooth vicinal surface into the hill-and-valley structure initiated by the adsorption of Au. With increasing substrate temperature from (a) to (d) the hill-and-valley structure becomes simpler: The structure is two dimensional as in (a) and (b) but more and more one dimensional as in (c) and (d). It is important for the interpretation of the images to consider the strong image distortion due to the foreshortening factor of 1/40! The superterraces [bright bands in (c) and (d)] are very straight and run almost perfectly along the ⟨110⟩ direction. It is surprising that the bands are almost straight over 300 μm and that such a well-ordered structure can be obtained by self-organization due to an adsorption-induced change of surface free energies.

The average period between the flat (001) terraces is quite similar in Figs. 14(a)–14(d): the separation between superterraces is about 400 nm. However, the average width of the dark bands, i.e., the step bands or facets increases with temperature. Wider dark bands (facets) correspond to lower inclination angle of the facets due to the conservation of the macroscopic miscut of 4°: The area of the flat (001) areas decreases with increasing facet area and decreasing facet angle. At an adsorption temperature of 880 °C the ratio of the (001) areas to the (119) facets is almost 1:1, which agrees well with a (119)-facet orientation. In (d) the average width of all facets is the same as the width of the (001) flat terraces indicating that almost all facets exhibit a (119) orientation. Formation of (117) and (115) facets is observed at lower temperatures in image (a) and (b).

The step bunching process is a kinetically limited process and is therefore governed by the deposition conditions of Au. At lower temperatures the length of the superterraces decreases due to reduced Si adatom diffusion and a large number of nucleation sites. The facet orientation also depends on adsorption temperature. At high temperatures most of the facets show the energetically favorable (119) orientation, with decreasing temperatures (117) and (115) orientations are observed. It should be pointed out, that these facets do not exhibit an Au-induced reconstruction, i.e., do not have the low surface free energy of the (119) facet.

The dark elliptical dots in Fig. 14(b) and 14(d) are 3D islands formed by excess Au deposition beyond the satura-

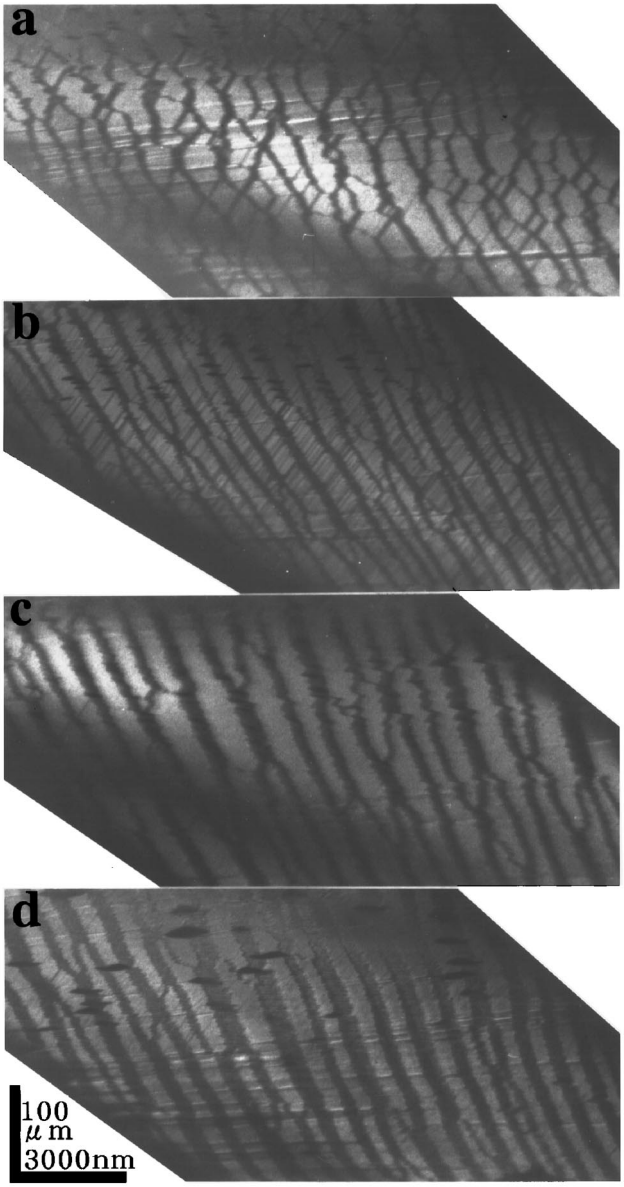

FIG. 14. Surface morphology after Au adsorption at various temperatures (a) 800, (b) 825, (c) 850, and (d) 880 °C in bright field imaging condition using REM. Field of view is 16 and 300 μm, respectively. Bright bands correspond to (001) superterraces, dark bands to facets. With increasing temperature the length of the structures exceeds 300 μm and the facets get wider.

tion coverage of the surface monolayer. The 3D islands preferentially nucleate on the facet areas. The faceting is not affected by the formation of 3D islands because the morphological changes are already complete when the clusters start to nucleate. Electromigration of 3D islands to the anode direction was also observed[21,22] and details will be described in elsewhere. This is in strong contrast to the case of Au deposition on the (*hhm*) surface with $m/h=1.4-1.5$, where the morphology of the hill-and-valley structure depend on the Au coverage.[6]

Figures 16(a) and 16(b) show the surface morphology with higher magnification after Au adsorption at 800 and 880 °C, respectively. Boundaries between the facets and the (001) terraces are zigzagged in shape in both images. Dark

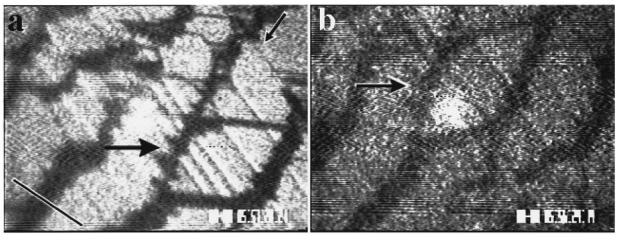

FIG. 15. REM image with higher magnification after Au adsorption at 825 °C: (a) bright field image condition using the specular spot. (b) dark field imaging condition using the (1/5 0) spot. The length of the scale bar is 300 nm.

lines in the flat (001) terraces are visible along two directions as indicated by arrows. The lines along the horizontal direction are parallel to the miscut direction (⟨110⟩ direction); the others are estimated to point in the $\langle 1\bar{1}0\rangle$ direction (considering the foreshortening factor of 1/40 and the azimuth misorientation of the incident beam from the $\langle 1\bar{1}0\rangle$ direction). The dark lines in the (001) terraces are very likely narrow minority domains with a 3.2×5 structure. Domain boundaries between 5×3.2 domains and 3.2×5 domains must be accompanied by steps along the ⟨110⟩ or the $\langle 1\bar{1}0\rangle$ direction. The boundaries between the (001) terraces and the facets are also along the ⟨110⟩ and the $\langle 1\bar{1}0\rangle$ direction. The existence of the ⟨110⟩ boundaries, which causes a deviation of the average direction of the dark facets bands from the $\langle 1\bar{1}0\rangle$ direction, is due to a slight azimuth misorientation of the 4° miscut from the perfect ⟨110⟩ direction, which is adjusted by a small number of kinks. The estimated value is about 1.9°, and an off angle to the $\langle 1\bar{1}0\rangle$ direction less than 0.1° exists.

Additional domain boundaries or steps are also observed in the dark facet areas. Due to the grazing incidence of the electron beam, i.e., the foreshortening factor of 1/40, the slight misorientation of the incident electron beam and the not exactly known orientation of the facet areas it is impossible to determine the orientation of these defects. Further detailed studies are necessary to determine the exact nature of these defects.

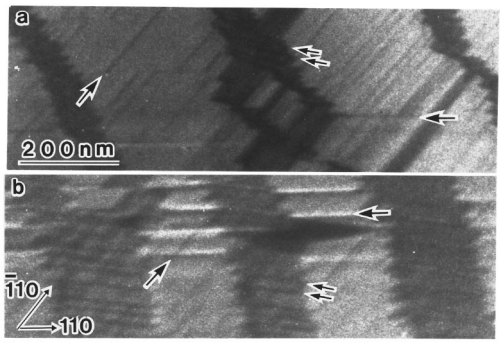

FIG. 16. Details of the domain structure on the (001) terraces and facets after Au adsorption become apparent in higher magnification. The REM images show the zigzag shape of the facet areas, domain boundaries as dark lines in the (001) terraces and also in the facet areas. (a) Au adsorbed at 800 °C gave (117) facets. (b) Au adsorbed at 880 °C produced (119) facets.

IV. SUMMARY

Au-adsorption-induced step bunching and faceting were studied by SPA-LEED and REM. These processes can be classified into four stages as follows. In stage 1 (from $t=0$ to $t=t_1$) no changes of surface morphology are observed. For stage 2 (form $t=t_1$ to $t=t_1'$) nucleation of the 5×3.2 structure on the (001) surface resulting in the formation of the step bands is observed. During stage 3 (from $t=t_1'$ to $t=t_2$) expansion of the (001) surface areas resulting in an increase of the slope of the step bands is observed. Finally in stage 4 (from $t=t_2$ to $t=t_3$) facet formation is observed.

Step bunching takes place due to the expansion of the Si(001)5×3.2-Au terraces because the surface free energy of the (001) areas is reduced by the formation of the 5×3.2 structure. The step bunching is a kinetic process and the step bands ultimately form facets. The driving force for the formation of such a hill-and-valley structure composed of Si(001)5×3.2-Au terraces and facets is the reduction of the surface free energy of the system.

Three kinds of facets ((119), (117), and (115) facets) were observed depending on the substrate temperature and the deposition rate. Under optimum conditions only (119) facets are formed but there is no temperature in the range between 750 and 845 °C at which only (117) facets are formed. Thus, the faceting of the (115), (117), and (119) planes seems to be related partly to kinetic processes. However, the (119) facet is the most stable because the 8×2 structure or the 4×2 structure is formed on the (119) surface. The formation of the hill-and-valley structure composed of the flat (001) terraces and the (119) facets is energetically favored.

The large-scale morphological transformation of a smooth 4° off Si(001) vicinal surface into a 1D terrace and facet structure during Au adsorption has been studied by *in situ* REM. Triggered by the formation of the Au-induced reconstruction on the Si(001) plane extremely elongated flat (001) terraces are formed with an average separation of 200–1000 nm and a length of more than 300 μm. Conservation of the number of steps, i.e., the macroscopic miscut requires the formation of the step bands that finally transform into well-ordered and well-oriented (119) facets that separate the (001) terraces.

ACKNOWLEDGMENTS

Fruitful discussions with Professor M. Heuzler are gratefully acknowledged. This work was supported by a Grant-in Aid from the Ministry of Education, Science and Culture (Nos. 07044133, 09650026, and 08NP1201) and the Deutsche Forschungsgemeinschaft (Ho1611/4-1).

*Author to whom correspondence should be addressed. Present address: Physics Department, Tokyo Institute of Technology, Oh-Okayama, Meguro, Tokyo 152, Japan. FAX: 81-3-5734 2079 Electronic address: hminoda@surface.phys.titech.ac.jp

[1] See, for example, S. Ino, *Reflection High-Energy Electron Diffraction and Reflection Electron Imaging of Surfaces*, edited by P. K. Larsen and P. J. Dobson, Vol. 188 of NATO Advanced Study Institute Series B: Physics (Plenum, New York, 1987), pp. 3–28.

[2] H. Minoda, Y. Tanishiro, N. Yamamoto, and K. Yagi, Surf. Sci. **331–333**, 913 (1995).

[3] E. Suliga and M. Henzler, J. Vac. Sci. Technol. A **1**, 1507 (1982).

[4] L. Seehofer, S. Huhs, G. Falkenberg, and R. L. Johnson, Surf. Sci. **329**, 157 (1995).

[5] M. Jalochowski, M. Strozak, and R. Zdyb, Surf. Sci. **375**, 203 (1997).

[6] K. Aoki, H. Minoda, Y. Tanishiro, and K. Yagi, Surf. Rev. Lett. **5**, 653 (1998).

[7] K. Aoki, T. Suzuki, H. Minoda, Y. Tanishiro, and K. Yagi, Surf. Sci. **408**, 101 (1998).

[8] T. Kamino, T. Yaguchi, M. Toimita, and H. Saka, Philos. Mag. A **75**, 105 (1997).

[9] T. Suzuki, Y. Tanishiro, H. Minoda, and K. Yagi, Surf. Sci. **298**, 473 (1993).

[10] Y. W. Mo, J. Kleiner, M. B. Webb, and M. G. Lagally, Phys. Rev. Lett. **66**, 1998 (1991).

[11] J. E. Griffith, G. P. Kochanski, J. A. Kubby, and P. E. Wierena, J. Vac. Sci. Technol. A **7**, 1914 (1989).

[12] B. S. Swartzentruber, M. B. Mo, M. B. Webb, and M. G. Lagally, J. Vac. Sci. Technol. A **7**, 2901 (1989).

[13] O. Alerhand, A. N. Becker, J. Joannopoulos, D. Vanderbilt, R. Hamers, and J. Demuth, Phys. Rev. Lett. **64**, 2406 (1990).

[14] M. Horn von Hoegen, H. Minoda, K. Yagi, F.-J. Meyer zu Heringdorf, and D. Kähler, Surf. Sci. **402–404**, 464 (1998).

[15] K. Yagi, Surf. Sci. Rep. **17**, 305 (1993).

[16] M. Horn von Hoegen, J. Falta, and M. Henzler, Thin Solid Films **183**, 213 (1989).

[17] K. Oura, Y. Makino, and T. Hanawa, Jpn. J. Appl. Phys. **15**, 737 (1976).

[18] X. F. Lin, K. J. Wan, J. C. Glueckstein, and J. Nogami, Phys. Rev. B **47**, 3671 (1993).

[19] G. Jayaram and L. Marks, Surf. Rev. Lett. **2**, 731 (1995).

[20] The mapping of the spots is determined by the intersection of the Ewald sphere with the reciprocal lattice. For normal incidence a LEED pattern is not distorted; for grazing incidence, however, a LEED pattern is distorted along the x axis.

[21] A. Yamanaka Y. Tanishiro, and K. Yagi, Surf. Sci. **264**, 55 (1992).

[22] T. Ichinokawa, C. Haginoya, D. Inoue, and H. Itoh, Phys. Rev. B **47**, 9654 (1993).